IX CONGRESSO BRASILEIRO DE ENGENHARIA E CIÊNCIAS TÉRMICAS
9th BRAZILIAN CONGRESS OF THERMAL ENGINEERING AND SCIENCES

Paper CIT02-0874

Mathematical model of a hybrid capillary pumped loop

Valeri V. Vlassov
Instituto Nacional de Pesquisas Espaciais – INPE, DMC, 12227-010, S.J.Campos, SP, Brasil
vlassov@dem.inpe.br

Abstract. ***A mathematical model of a hybrid capillary pumped loop (CPL) with two reservoirs (attached to and separated from evaporator) was developed. Selected configuration includes features of a generic CPL with controlled reservoir and of a loop heat pipe with compensation chamber. In the developed model the momentum and mass balance equations are coupled at microscopic and macroscopic (system) levels. Correspondingly, there are two hierarchic parts of model with inter-level interfacing. Such kind of models is introduced as imitation ones, due to potential capability to simulate various operational modes of the device including switching to some failure modes. The main assumption is the shape of interface surfaces can be predicted a priory as a function of given geometry of voids and its rate of flooding with liquid. It allows the performing of tracking of interfaces motion at system level. All mechanisms causing an interface to move were considered: evaporation-condensation, flooding-recession and thermal expansion-contraction. At system level, an equivalent hydraulic network of dynamic structure was established. Interaction between these two levels was accomplished the boundary conditions of microscopic model. The main purpose of the paper is to introduce a new type of the CPL model; therefore no closed numerical algorithm was developed. Nevertheless, some discrete analogous and recommendations for shifting up the variables to the higher time layer were presented.***

Keywords. *Capillary pumped loop, Loop heat pipe, interface tracking, mathematical model*

Nomenclature

A	section area or interface area (m^2)
C	specific heat (J/kg/K)
f	density of viscosity forces ($kg/m^2/s^2$)
$\bar{f}$	density of mass forces ($kg/m^2/s^2$)
h	heat transfer coefficient ($W/C/m^2$)
h_r	recession (m)
j	mass flow density ($kg/s/m^2$)
K	permeability ($1/m^2$)
k	thermal conductivity (W/m/C)
L	length (m)
$\dot{m}$	mass flow rate (kg/s)
P	pressure (Pa)
q	heat flux density (W/m^2)
R, r	radius (m)
R''	gas constant for vapor (J/kmole/K)
s	interface position (m)
$\dot{s}$	moving interface velocity (m)
T	temperature (K)
u	velocity along characteristics (m/s)
V	volume (m^3)
v	radial velosity (m/s)
w	velocity along axis (m/s)
y	characteristics (m)
z	coordinate (m)

Greeks

δ	Boolean variable
	small variation
ε	porosity
	emissivity
λ	latent heat of evaporation (J/kg)
μ	dynamic viscosity (Pa s)
θ	wetting angle
ρ	density (kg/m^3)
σ	liquid surface tension (N/m)
	Stefan-Boltzman constant ($W/m^2/K^4$)

Subscripts

''	vapor phase
^	higher time layer
p	pore
w	wick
'	liquid phase

1. Introduction

Capillary Pumped Loops (CPL) and Loop Heat Pipes (LHP) are two-phase heat-transport devices, which rely on the surface-tension forces induced by a fine pore wick to drive a working fluid. These devices use the same principle like widely known heat pipes, i.e. closed evaporation-condensation cycle being maintained by capillary pumping.

Because of their grand potential heat transport efficiency, these devices are emerging as the baseline design of thermal control systems for space applications. CPL were invented in USA (NASA) in late 60's (Stenger, 1966) whereas LHP (that is a type of CPL) appeared in Russia in early 70's (Gerasimov, Maidanik, at al, 1976 and 1985). Maidanik in 1997, Nikitkin in 1998 and Ku in 1999 did a review of CPL and LHP, and their similarities and differences. LHP and CPL are the baseline design for thermal control in GLAS, EOS-Chemistry, GOES, SWIFT spacecraft and several communications satellites.

Both types of CPL have a cylindrical fine pore evaporator and a tube-type condenser, which provides a necessary liquid subcooling to avoid vapor phase formation in the liquid core of evaporator during operation. The CPL has a reservoir as a separate element having a hydraulic link to the liquid line whereas the LHP compensation chamber is incorporated in the evaporator. Main functions of the reservoir is to accommodate volume variations of liquid phase in the condenser because of the liquid-vapor interfaces motion in respond of variations in applied heat power or environment conditions. The CPL reservoir also is used for active control and pre-conditioning on start-up. Properly sized compensation chamber in LHP provides a vapor-tolerant operation mode of evaporator; liquid density variation over temperature at cold and hot cases of environment extremes should be taken into account. Proposed in this paper a hybrid CPL configuration combines features of both types of a reservoir and potentially can present reliable start-up characteristics and good control-ability as well. This type of CPL still has not been well studied.

Although the CPL and LHP technologies have reached a high level of maturity, many issues still remain as subjects of active research. The reason lies in a complex coupled heat-hydraulic behavior of two-phase fluid inside. It presents several operation modes and possible failures, like eventual evaporator dry-out, degradation of characteristics, pressure oscillations, etc. These modes and failures actually are studied experimentally due to lack of representative mathematical models. For example, start-up problems have been investigated by Butler and Hoang in 1991, Ku at al. in 1996 and others. High frequency pressure oscillations were detected and investigated in 1995 by O'Connell, at al, Ku at al, Hoang, at al. Kiper at al in 1988 and Kolos at al in 1997 studied the low frequency oscillations. Maidanik at al, in 1993 reveals the low power limit. There were several flight missions carrying CPL as scientific payloads and devoted to investigations of its performance under micro-gravity (Butler, at al, 1995 and 1996; Antoniuk at al, 1998).

Each operational or contingency mode is related to one or a combination of internal thermo-hydraulic processes that takes place in a CPL. The list of possible inside physical processes in a CPL is presented below (in alphabetic order).

- Condensation on interface at any location
- Evaporation from inside of the wick bulk
- Evaporation from interface at any location
- Eventual condensation in vapor line
- Eventual liquid back flow
- Eventual vapor back flow
- Flooding of evaporator grooves
- Interface motion in condenser tube
- Lateral priming of primal wick from compensation chamber in evaporator
- Liquid motion through secondary wick in evaporator
- Slug two-phase flow
- Vapor bubble formation and collapse in the liquid channel of evaporator
- Vapor bubbles formation in flooded vapor grooves of evaporator.
- Vapor penetration in wick bulk
- Variation of vapor void volume in compensation chamber and reservoir
- Wick progressive dry-out

To simulate a whole spectrum of operational and non-operational modes, the mathematical model of a CPL should adequately represent the most of the listed processes. Theoretical studies at the present are lagged behind the experimental ones. The mathematical models were developed either at microscopic level with well-defined fixed boundary conditions, or at system level, using the node-type simplified discretization. Cao and Faghri in 1994 developed model for element of CPL evaporator; Khrustalev and Faghri in 1995 investigated evaporation from meniscus of porous wicks; Figns at al. in 1999 completed researches on evaporation from evaporator bulk of a CPL. Muraoka and Vlassov (2000) elaborated a node-model for a CPL space experiment; Cullimore (2000) developed a most advanced node-type model of LHP, which was incorporated into the SINDA/Fluint fluid-thermal analyzer software.

Majority of developed models simulate the normal mode of operation, steady state or transient. But the point of practical interest for a designer is rather the switching between operational modes under smooth variation in external conditions and recuperation proceeding after failures. Corresponding internal boundary conditions are moving liquid-vapor interfaces, which may also eventually disappeared or appeared. Thus, an investigation should be done toward a creation of a special mathematical model of variable structure, variable number of interfaces and boundary conditions. This mathematical model must be capable to simulate most of possible internal processes as well as inter-switching between them. Such a model has to have a mechanism for tracking of interface positions and simulate its motions in respond to variations of external conditions.

This type of a model can be introduced as "imitation mathematical model - IMM". Imitative modeling of two-phase devices is a new approach in theoretical investigation for CPL. Investment in this direction can have a great practical importance. New results can be obtained using the IMM, that may give an important design instrument that is capable to

simulate the real operation of a device under all spectrum of external conditions and internal phase distributions that may occurs during a space vehicle mission.

This work is an attempt to make a step toward creating a IMM based on the proposed configuration of a hybrid CPL with two reservoirs. The emphasis was done toward the describing of the mechanism of moving interfaces at macroscopic (system) level, presentation of equivalent hydraulic network as a dynamic structure and developing of the model at two hierarchic levels. A mathematical model once created for the hybrid configuration, can be easy adapted to either LHP or generic CPL.

2. Theoretical fundamentals

The approach is to perform modeling at two hierarchic levels with certain algorithm of interacting. The low level sub-model is a generic set of momentum, mass and energy balance equations, where the liquid-vapor interfaces are defined through the high-level model and are taken as boundary conditions for the low level.

The high level model consists of sets of mass and motion conservation equations, which defines movement of the vapor-liquid interfaces over the internal volumes of the system. The balance equations take into account surfaces and mass forces acting on moving liquid slugs, as well as thermal expansion-contraction of working liquid. Temperature maps are obtained from the low-level sub-model.

Let consider a liquid slug trapped in a free-shape network with axis symmetrical channels (branches) of variable cross sections, see Figure 1. A set of curvilinear characteristics $(O_i\text{-}Y_i)$ with distinct origins can be established. S_i is a current imaginary position of the i-th interface on the $(O_i\text{-}Y_i)$ characteristic or its origin. The interface position is defined with respect to a mid-cross-section determined by integration over the interface surface in the suggestion that it has a specific curvature. An equivalent hydraulic network is shown at right side of the Figure 1.

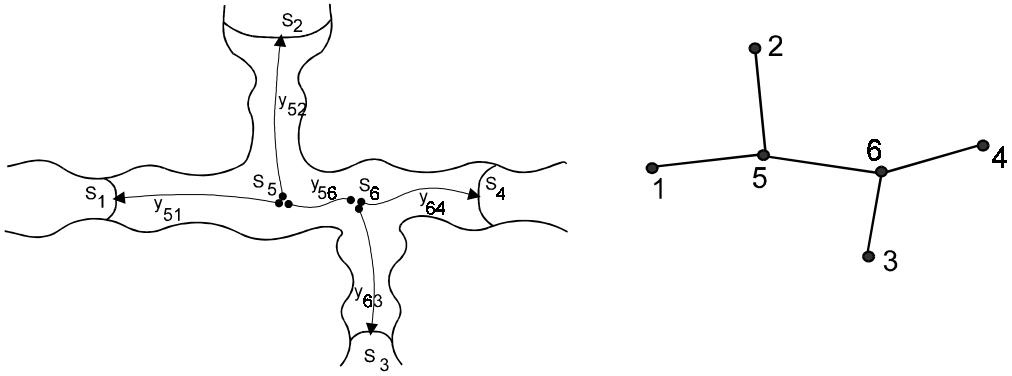

Figure 1. Liquid slug trapped in a network and its hydraulic equivalent

Let express a small variation of the mass integral over the slug with time δt. First, at time t, the mass is

$$m(t) = \sum_{(i \cap j)=1}^{N_n} \int_{s_i}^{s_j} A\rho dy_{ij} \tag{1}$$

Where N_n is a total number of nodes in the equivalent hydraulic network.
At the time $t+\delta t$, the total mass of the trapped liquid will be as following

$$m(t+\delta t) = \sum_{(i \cap j)=1}^{N_n} \int_{s_i}^{s_j+\delta s_j} A(\rho+\delta\rho) dy_{ij} \tag{2}$$

The integral can be evaluated as following

$$\int_{s_i}^{s_j+\delta s_j} A(\rho+\delta\rho)dy_{ij} = \int_{s_i}^{s_j} A\rho dy_{ij} + \int_{s_i}^{s_j+\delta s_j} A\rho dy_{ij} + \int_{s_i}^{s_j} A\delta\rho dy_{ij} + \int_{s_i}^{s_j+\delta s_j} A\delta\rho dy_{ij} \approx$$
$$\int_{s_i}^{s_j} A\rho dy_{ij} + \int_{s_i}^{s_j} A\delta\rho dy_{ij} + A(s_j)\rho(s_j)\delta s_j \tag{3}$$

The variation of liquid total mass with time is defined by evaporation-condensation balance over all interfaces

$$\frac{\partial m}{\partial t} \cong \frac{m(t+\delta t)-m(t)}{\delta t} = -\sum_{j=1}^{N_{if}} j_j A(s_j) \tag{4}$$

Where N_{if} is a total number of interfaces $(N_{if} \le N_n)$. After transformation to derivative,

$$\sum_{j=1}^{N_{if}} \rho(s_j) A(s_j) \frac{\partial s_j}{\partial t} + \sum_{(i \cap j)=1}^{N_n} \int_{s_i}^{s_j} A \frac{\partial \rho}{\partial t} dy_{ij} = -\sum_{j=1}^{N_{if}} j_j A(s_j) \tag{5}$$

A quasi one dimensional (1D) mode motion was assumed in each branch of a hydraulic network. Particular case when all fluxes $j_j=0$ is the non-operational mode.

The density of liquid can be approximated by a polynomial function, as it depends of temperature: $\rho = \rho_0 + \alpha T + \beta T^2$. Finally, for the liquid slug, the mass balance equation is the following

$$\sum_{(i \cap j)=1}^{N_n} \int_{s_i}^{s_J} A(\alpha + \beta T) \frac{\partial T}{\partial t} dy_{ii} + \sum_{j=1}^{N_{if}} \rho(s_i) A(s_i) \dot{s}_i = -\sum_{j=1}^{N_{if}} j_j A(s_j) \tag{6}$$

Where temperatures and its derivatives come from energy equations at low level.

This equation of mass conservation for an entire liquid slug yields important constraint for the relative motions of interfaces. It combines three mechanisms of liquid motion: first, due to liquid thermal expansion (first term); second, due to interface motion (second term) taking into account cross-area changes at interfaces positions; and third, due to integral balance over evaporation-condensation rates from all interfaces (right part). Particular balance for each branch with interface can be extracted from the general equation

$$\int_{s_i}^{s_j} A(\alpha + \beta T) \frac{\partial T}{\partial t} dy_{ij} + \rho(s_j) A(s_j) \dot{s}_j = \dot{m}_{ij} - j_j A(s_j) \tag{7}$$

As soon as the mass flow rates for branches were introduced ($\dot{m}_{ij}$), the input-output mass flow balance must be fulfilled in the hydraulic nodes, which are not interfaces:

$$\sum_{i \in J_i} \dot{m}_{ij} \equiv \sum_{i \in J_i} (A \rho u)_{ij} = 0, \qquad j = 1,\ldots,(N_n - N_{if}) \tag{8}$$

Where J_i is a set of numbers of the nodes linked to the *i*-th node; the sign is opposite for entering and exiting flows. There is all for the mass balance on system level.

To create a set of the motion equations let write a momentum balance along the characteristic for each branch of the network-type system. As a base, a motion equation in classic Euler form can be used

$$\frac{\partial(\rho u)}{\partial t} + \frac{\partial(\rho u^2)}{2\partial y} = -\frac{\partial P}{\partial y} + f_{iy} + \bar{f}_{iy} \tag{9}$$

The derivative of the mass flow rate can be expressed as the following

$$\frac{\partial \dot{m}_{ij}}{\partial t} = \frac{\partial(\rho A u)_{ij}}{\partial t} = \rho u_{ij} \frac{\partial A}{\partial t} + A \frac{\partial(\rho u)_{ij}}{\partial t} = \rho u_{ij}^2 \frac{\partial A}{\partial y_{ij}} + A \frac{\partial(\rho u)_{ij}}{\partial t} \tag{10}$$

Hereafter it will be meant that densities ρ and cross-areas A have a subscript (ij), if other is not mentioned. Multiplying the motion equation by A and substituting the last into it, one can obtain

$$\frac{\partial(\rho A u)_{ij}}{\partial t} + A\frac{\partial(\rho u^2)_{ij}}{2\partial y_{ij}} - \rho u_{ij}^2 \frac{\partial A}{\partial y_{ij}} = -A\frac{\partial P}{\partial y_{ij}} + A\ f_{ij} + A\bar{f}_{ij} \tag{11}$$

Or, transferring to the mass flow rate variables

$$\frac{\partial \dot{m}_{ij}}{\partial t} + \frac{1}{2}\dot{m}_{ij}\frac{\partial u_{ij}}{\partial y_{ij}} - \frac{3}{2}\rho u_{ij}^2 \frac{\partial A}{\partial y_{ij}} = -A\frac{\partial P}{\partial y_{ij}} + Af_{ij} + A\bar{f}_{ij} \tag{12}$$

Mass balance over a branch gives

$$\frac{\partial \dot{m}_{ij}}{\partial y_{ij}} = \frac{\partial(u\rho A)_{ij}}{\partial y_{ij}} = \rho A\frac{\partial u_{ij}}{\partial y_{ij}} + u_i\frac{\partial(\rho A)_{ij}}{\partial y_{ij}} = 0 \tag{13}$$

After dividing again by A, the integration along a characteristic y_i can be performed Thus, the integral of the second term of the momentum balance equation can be expressed as following

$$\frac{1}{2}\dot{m}_{ij}\int_{s_i}^{s_j}\frac{1}{A}\frac{\partial u_{ij}}{\partial y_{ij}}dy_{ij} = \frac{1}{2}\dot{m}_{ij}\int_{s_i}^{s_j}\frac{1}{A}\left(-\frac{u_{ij}}{\rho A}\frac{\partial(\rho A)_{ij}}{\partial y_{ij}}\right)dy_{ij} = \frac{1}{2}\dot{m}_{ij}^2\int_{s_i}^{s_j}\frac{1}{A}\left(-\frac{1}{(\rho A)^2}\frac{\partial(\rho A)}{\partial y_{ij}}\right)dy_{ij} \tag{14}$$

The third term is

$$-\frac{3}{2}\int_{s_i}^{s_j}\frac{\rho u_{ij}^2}{A}\frac{\partial A}{\partial y_{ij}}dy_{ij} = -\frac{3}{2}\int_{s_i}^{s_j}\frac{\dot{m}_{ij}^2}{\rho A_{ij}^3}\frac{\partial A}{\partial y_{ij}}dy_{ij} = \frac{1}{2}\dot{m}_{ij}^2\int_{s_i}^{s_j}\frac{(-3)}{\rho A^3}\frac{\partial A}{\partial y_{ij}}dy_{ij} \tag{15}$$

Finally,

$$\frac{\partial \dot{m}_i}{\partial t}\psi_1(s_j) + \frac{1}{2}\dot{m}_{ij}^2\psi_2(s_j) = P(s_i) - P(s_j) + \int_{s_i}^{s_j} f_{ij}dy_{ij} + \int_{s_i}^{s_j}\bar{f}_{ij}dy_{ij} \tag{16}$$

Where the two interface form-functions are defined as

$$\psi_1(s_j) = \int_{s_i}^{s_j}\frac{dy_{ij}}{A}; \qquad \psi_2(s_j) = -\int_{s_i}^{s_j}\frac{4}{\rho A^3}\frac{\partial A}{\partial y_{ij}}dy_{ij} - \int_{s_i}^{s_j}\frac{1}{\rho^2 A^2}\frac{\partial \rho}{\partial y_{ij}}dy_{ij} \tag{17}$$

Note, these functions are completely defined by the branch geometry and liquid properties, and in the case of simple shapes the integration can be performed analytically. If density is not a function of temperature, the second function consists only of the first component.

For example, for the flow along the z-axis of a tube of constant diameter D,

$$\psi_1(z) = \frac{4(z - z_0)}{\pi D}; \qquad \psi_2(z) = 0. \tag{18}$$

For the flow along the radius R of a cylinder of the length B ($\rho \neq \rho(T)$):

$$\psi_1(R) = \frac{1}{2\pi B}\ln\left(\frac{R}{R_0}\right); \qquad \psi_2(R) = -\frac{1}{\rho\pi^2 B^2}\left[\frac{1}{2R_0^2} - \frac{1}{2R^2}\right]. \tag{19}$$

The viscous losses term in general case can be expressed by such a manner that the mass flow rate and geometrical-viscosity component can be separated

$$\int_{s_i}^{s_j} f_{ij}\,dy_{ij} = \dot{m}_{ij}\left|\dot{m}_{ij}\right|^a \int_{s_i}^{s_j} \tilde{f}_{ij}(s_j,\mu,A)\,dy_{ij} \tag{20}$$

The kernel function can be derived either from experimental data obtained for similar channels or by solution of 2D-3D Navier-Stokes equations at the low level. The numerical equivalent of the momentum balance equations can be written as the following

$$\frac{\hat{\dot{m}}_{ij} - \dot{m}_{ij}}{\Delta t}\psi_1(s_j) + \frac{1}{2}\hat{\dot{m}}_{ij}\dot{m}_{ij}\psi_2(s_j) = P(s_i) - P(s_j) + \hat{\dot{m}}_{ij}\left|\dot{m}_{ij}\right|^a \int_{s_i}^{s_j} \tilde{f}_{ij}(s_j,\mu,A)\,dy_{ij} + \int_{s_i}^{s_j} \bar{f}_{ij}\,dy_{ij} \tag{21}$$

Linear component of mass flow rate was accepted as one for higher time layer, and rest - for current time layer. It allows linear expressing the mass flow rates through pressures in hydraulic nodes of the network.

$$\hat{\dot{m}}_{ij} = \alpha_{ij}P(s_i) - \beta_{ij}P(s_j) + \gamma_{ij} \tag{22}$$

Where coefficients α,β,γ are functions of mass flow rate at the current time layer, interface position, liquid viscosity and channel geometry and are the subject for afterward-iterative adjustment.

This expression can be substituted into the nodal mass flow balances. It gives a set of linear equations with respect to pressures in the internal nodes. For example, for the network presented in the Figure 1, it give two equations with respect to $P(s_5)$ and $P(s_6)$. It is assumed, that pressure at interfaces $P(s_i)$, i=1,2,3,4, are known or already calculated from other equations. Total number of such equations is $(N_n\text{-}N_{if})$: 6-4=2.

The equation for the mass flow rate can be substituted in the branch mass balance equation. After numerical representation it gives

$$\int_{s_i}^{s_j} A(\alpha+\beta T)\frac{\partial T}{\partial t}\,dy_{ij} + \rho(s_j)A(s_j)\frac{\hat{s}_j - s_j}{\Delta t} = \alpha_{ij}P(s_i) + \gamma_{ij} - \frac{\partial(j_j A(s_j) + \beta_{ij}P(s_j))}{\partial s_j}(\hat{s}_j - s_j) \tag{23}$$

Note, the components $j_j\dfrac{\partial A(s_j)}{\partial s_j}$ and $\beta_{ij}\dfrac{\partial P(s_j))}{\partial s_j}$ are rather geometrical characteristics whose expressions can be obtained a priori. Weak links with other variables can be treated explicitly.

Each of this equation can be treated separately; an iterative adjustment with respect to interface positions is needed. Total number of such equations is N_{if}.

Evaporation-condensation rate over each interface is expressed via pressures and current temperatures (Faghri, 1995):

$$j_i = \frac{2\alpha}{(2-\alpha)}\sqrt{\frac{1}{2\pi R''}}\cdot\left[\frac{P_{sat}(T_i)}{\sqrt{T_i}} - \frac{P_i''}{\sqrt{T_i''}}\right] \tag{24}$$

The last is a part of the set of energy balance equations and should combine with the equations for vapor phase volumes

$$V_i'' \frac{\partial P_i''}{\partial t} - P_i'' V_i'' \frac{\partial \ln T_i''}{\partial t} + P_i'' \frac{\partial V_i''}{\partial t} = \int_{A_i} j_i dA_i \qquad (25)$$

Where the integration should be performed over interfaces surrounding the given *i*-th vapor volume.
This equation was derived from the ideal gas relationship.

3. Hybrid CPL configuration

The hybrid CPL is suggested as a baseline LHP configuration with an additional separate reservoir, similar to that of a generic CPL, for improving the loop control capability. The LHP's compensation chamber is named here as an attached reservoir, having a capillary link to the primal wick of the evaporator. Besides of two reservoirs, the hybrid CPL consists of cylindrical evaporator with a fine-pore wick, two vapor and liquid pipelines which form a tube condenser.

The attached reservoir is used to store excess liquid. A capillary link with primal wick ensures that the evaporator wick is always wetted. This means the loop can be started any time by simply applying power to the evaporator, eliminating any requirements of pre-conditioning.

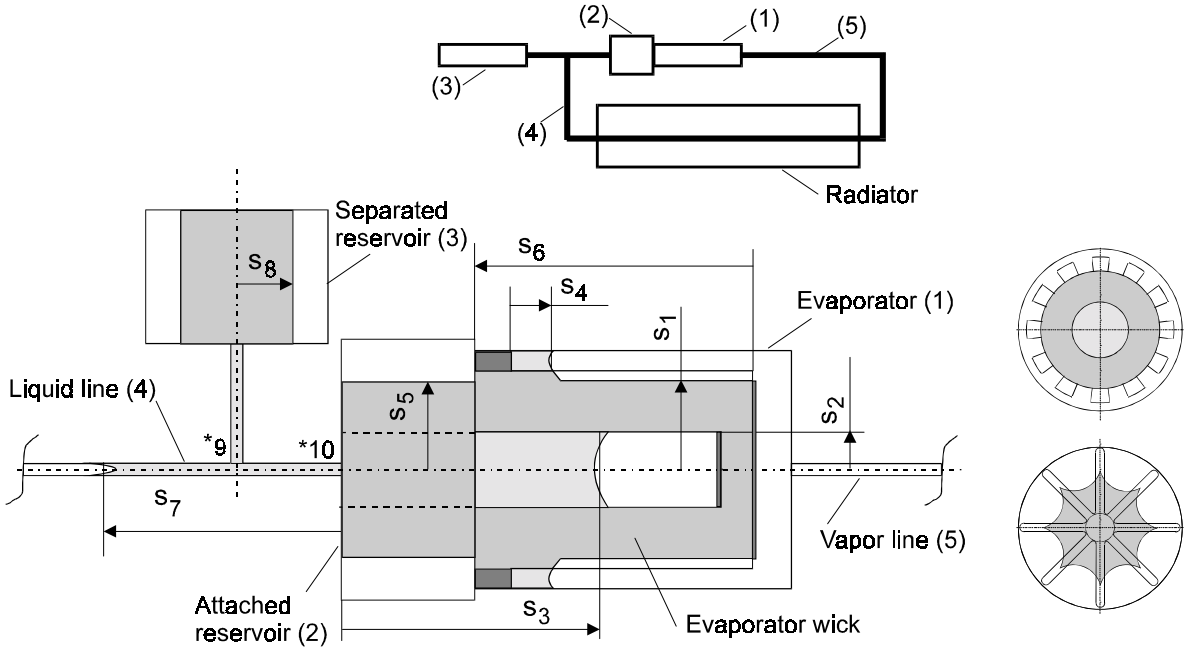

Figure 2. The hybrid CPL configuration with interfaces distribution corresponding to a possible start-up mode; the evaporator and reservoirs configurations.

The separated reservoir is used for controlling the CPL heat transfer capability in respond to alterations in external conditions and applied heat load on evaporator. If the reservoir temperature will be maintained at a constant level, the interface in it will interact with interface of condenser by such a manner that in case of heat loads decreasing, excess of liquid will occupied a major part of the condenser, its temperature decreases and rejected heat flux decreases. And opposite if heat load increases.

When design, the reservoir dimensions and amount of liquid to fill should be chosen by such a manner that there is a certain amount of liquid remaining in attached reservoir at any circumstance. Liquid density variation over temperature at the hot and cold cases of environment extremes must be taken into account.

The Figure 2 demonstrates this basic conception with indication of a possible position of the liquid-vapor interfaces in the device. The presented configuration corresponds a start-up mode, when vapor canal of evaporator can be partially flooded with liquid (interface s_4) and liquid return channel in the wick core can have a trapped vapor bubble (interface s_3).

The temperature of the attached reservoir approximately follows the evaporator temperature, being slightly below it with a certain time delay. The temperature of the separated reservoir can be easy stabilized and controlled by an electric heater. The interface s_8 will interact with the condenser interface s_7, realizing the self-control capability.

At the right of the Figure 2 the configuration of evaporator and both reservoirs are shown. In the reservoir an additional mesh-wick porous structure maintains vapor-liquid interface by such a manner that in 0-gravity conditions the separation of phases and dislocation of vapor phase to outer regions of the cylindrical reservoir takes place.

4. High level model

To perform a higher-level modeling, an equivalent hydraulic network should be created. This network for the start-up mode is shown in Figure 3. Nodes 1-8 are the moving liquid-vapor interfaces; nodes 9-10 are the liquid phase intermediate nodes; nodes 11-14 are pure vapor-volume (voids) nodes. Links between interface nodes and vapor ones reflect evaporating-condensing processes. Hydraulic links between interfaces mean that eventual moving of one interface can provoke moving of another interface. For example, eventual central bubble volume reduction (positive moving of s_3) will certainly cause increasing of vapor cavity in the attached reservoir (negative moving of s_5). On switch-off, the bubble will growth and can cause flooding of the vapor channel (a positive moving of s_4). In general case eventual moving of any interface can influence another one, or several of them, or all of them. Therefore, all interfaces in the equivalent network should be linked.

Important to note, the network has to have a dynamic structure, it means that in depend of the CPL operation mode some of interfaces can disappear. For example, if mentioned core bubble eventually will collapsed, the nodes 2,3 and 14 should be disappeared as well as links to them.

To treat such a dynamic structure an approach of generalized scheme can be utilized. Each node and its links is set to corresponded Boolean variables (δ) having values either 0 or 1. This network should display all possible combination of interface positions to reflect various operational modes.

Shown in Figure 3, the hydraulic network can be accepted as a generalized scheme. It can represent several operational modes, as well as a start-up mode, switch-off mode and re-start mode.

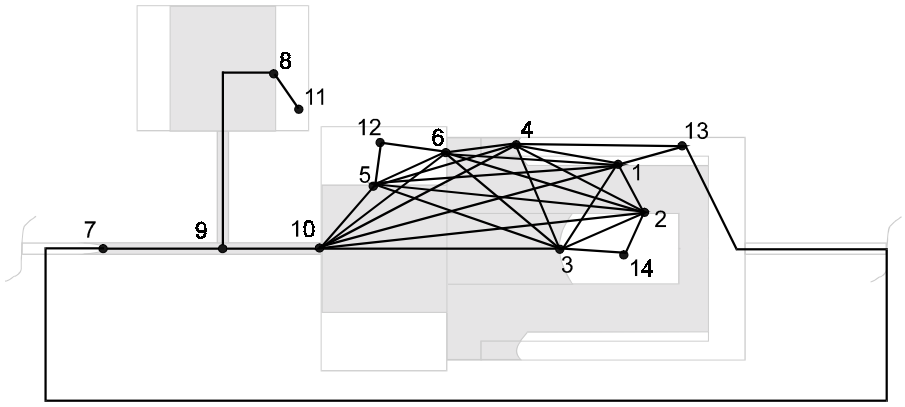

Figure 3. Equivalent hydraulic network for start-up configuration

Mass conservation over such a system under not-operating conditions is constant quantity of charged fluid (m_0) inside. The initial interfaces position should be adjusted by this condition:

$$\int_V \rho dV = \int_{V'} \rho dV' + \int_{V''} \rho'' dV'' = \sum_{(i \cap j)=1}^{14} \int_{s_i}^{s_j} A(\rho + \rho'') dy_i = m_0 \tag{26}$$

Mass balance on moving interfaces 1-6,8 can be written with involving of the Boolean variables:

$$\delta_1 \left(\rho A_1 \frac{\hat{s}_1 - s_1}{\Delta t} = -\hat{j}_{1-13} A_1 + \hat{\dot{m}}_{2-1} + \hat{\dot{m}}_{3-1} + \hat{\dot{m}}_{4-1} + \hat{\dot{m}}_{5-1} + \hat{\dot{m}}_{6-1} + \hat{\dot{m}}_{10-1} + \Delta \dot{m}_1 \right) \tag{27}$$

$$\delta_2 \left(\rho A_2 \frac{\hat{s}_2 - s_2}{\Delta t} = -\hat{j}_{2-14} A_2 + \hat{\dot{m}}_{1-2} + \hat{\dot{m}}_{3-2} + \hat{\dot{m}}_{4-2} + \hat{\dot{m}}_{5-2} + \hat{\dot{m}}_{6-2} + \hat{\dot{m}}_{10-2} + \Delta \dot{m}_2 \right) \tag{28}$$

$$\delta_3 \left(\rho A_3 \frac{\hat{s}_3 - s_3}{\Delta t} = -\hat{j}_{3-14} A_3 + \hat{\dot{m}}_{1-3} + \hat{\dot{m}}_{2-3} + \hat{\dot{m}}_{4-3} + \hat{\dot{m}}_{5-3} + \hat{\dot{m}}_{6-3} + \hat{\dot{m}}_{10-3} + \Delta \dot{m}_3 \right) \tag{29}$$

$$\delta_4 \left(\rho A_4 \frac{\hat{s}_4 - s_4}{\Delta t} = -\hat{j}_{4-13} A_4 + \hat{\dot{m}}_{1-4} + \hat{\dot{m}}_{2-4} + \hat{\dot{m}}_{3-4} + \hat{\dot{m}}_{5-4} + \hat{\dot{m}}_{6-4} + \hat{\dot{m}}_{10-4} + \Delta \dot{m}_4 \right) \tag{30}$$

$$\delta_5 \left(\rho A_5 \frac{\hat{s}_5 - s_5}{\Delta t} = -\hat{j}_{5-12} A_5 + \hat{\dot{m}}_{1-5} + \hat{\dot{m}}_{2-5} + \hat{\dot{m}}_{3-5} + \hat{\dot{m}}_{4-5} + \hat{\dot{m}}_{6-5} + \hat{\dot{m}}_{10-5} + \Delta \dot{m}_5 \right) \tag{31}$$

$$\delta_6\left(\rho A_6\frac{\hat{s}_6-s_6}{\Delta t}=-\hat{j}_{6-12}A_6+\hat{\dot{m}}_{1-6}+\hat{\dot{m}}_{2-6}+\hat{\dot{m}}_{3-6}+\hat{\dot{m}}_{4-6}+\hat{\dot{m}}_{5-6}+\hat{\dot{m}}_{10-6}+\Delta\dot{m}_6\right) \quad (32)$$

$$\delta_8\left(\rho A_8\frac{\hat{s}_8-s_8}{\Delta t}=-\hat{j}_{8-11}A_8+\hat{\dot{m}}_{9-8}+\Delta\dot{m}_8\right) \quad (33)$$

Where Δm_i is an additional term for the liquid thermal expansion. For the 1st interface it can be expressed as

$$\begin{aligned}\Delta\dot{m}_1=&\delta_2\left(\sum_{q=1}^{N_{s21}}\int_{s_2}^{s_1}A(\alpha+\beta T)\frac{\partial T}{\partial t}dy_{2-1,q}\right)+\delta_3\left(\sum_{q=1}^{N_{s31}}\int_{s_3}^{s_1}A(\alpha+\beta T)\frac{\partial T}{\partial t}dy_{3-1,q}\right)+\\&\delta_4\left(\sum_{q=1}^{N_{s41}}\int_{s_4}^{s_1}A(\alpha+\beta T)\frac{\partial T}{\partial t}dy_{4-1,k}\right)+\delta_5\left(\sum_{q=1}^{N_{s51}}\int_{s_5}^{s_1}A(\alpha+\beta T)\frac{\partial T}{\partial t}dy_{5-1,q}\right)+\\&\delta_6\left(\sum_{q=1}^{N_{s61}}\int_{s_6}^{s_1}A(\alpha+\beta T)\frac{\partial T}{\partial t}dy_{6-1,q}\right)+\sum_{q=1}^{N_{s10,1}}\int_{s_{10}}^{s_1}A(\alpha+\beta T)\frac{\partial T}{\partial t}dy_{10-1,q}\end{aligned} \quad (34)$$

Where N_{sij} is an overall number of streamlines, which begin from the surface s_i and come to the interface surface s_j. If a spatial numerical grid is applied to evaporator-reservoir for modeling, the integration along the streamlines y_i can be performed numerically too. These streamlines can be created from the velocity map, obtained numerically at each time step. The final expression and algorithm will be shown later, in the inter-model interfacing section.

The equations for the thermal expansion terms for 2,3,4,5,6, and 8 interfaces are similar. Correspondingly $\hat{\dot{m}}_{i-j}=-\hat{\dot{m}}_{j-i}$.

Thermodynamic-mass balances for the vapor volumes 11-14 are

$$\delta_8\left(V''_{11}(s_8)\frac{\hat{P}''_{11}-P''_{11}}{\Delta t}-P''_{11}V''_{11}(s_8)\frac{\hat{T}''_{11}-T''_{11}}{T''_{11}\Delta t}+P''_{11}\frac{V''_{11}(\hat{s}_8)-V''_{11}(s_8)}{\Delta t}=j_{8-11}A_8(s_8)\right) \quad (35)$$

$$\delta_5\left(V''_{12}(s_5)\frac{\hat{P}''_{12}-P''_{12}}{\Delta t}-P''_{12}V''_{12}(s_5)\frac{\hat{T}''_{12}-T''_{12}}{T''_{12}\Delta t}+P''_{12}\frac{V''_{12}(\hat{s}_5)-V''_{12}(s_5)}{\Delta t}=j_{5-12}A_5(s_5)+j_{6-12}A_6(s_5)\right) \quad (36)$$

$$\delta_4\left(V''_{13}(s_4)\frac{\hat{P}''_{13}-P''_{13}}{\Delta t}-P''_{13}V''_{13}(s_4)\frac{\hat{T}''_{13}-T''_{13}}{T''_{13}\Delta t}+P''_{13}\frac{V''_{13}(\hat{s}_4)-V''_{13}(s_4)}{\Delta t}=j_{1-13}A_1(s_4)+j_{4-13}A_4-\dot{m}_{13-7}\right) \quad (37)$$

$$\delta_3\left(V''_{14}(s_3)\frac{\hat{P}''_{14}-P''_{14}}{\Delta t}-P''_{14}V''_{14}(s_3)\frac{\hat{T}''_{14}-T''_{14}}{T''_{14}\Delta t}+P''_{14}\frac{V''_{14}(\hat{s}_3)-V''_{14}(s_3)}{\Delta t}=j_{2-14}A_2(s_3)+j_{3-14}A_3\right) \quad (38)$$

Where the evaporation-condensation rates are

$$\hat{j}_{i-j}=\frac{2\alpha}{(2-\alpha)}\sqrt{\frac{1}{2\pi R''}}\cdot\left[\frac{P_{sat}(\hat{T}_i)}{\sqrt{\hat{T}_i}}-\frac{\hat{P}''_j}{\sqrt{T''_j}}\right] \quad (39)$$

The non-linear term can be linearized around current temperature

$$\frac{P_{sat}(\hat{T}_i)}{\sqrt{\hat{T}_i}}=\frac{P_{sat}(T_i)}{\sqrt{\hat{T}_i}}\exp\left[\frac{\lambda M}{R_u}\left(\frac{1}{T_i}-\frac{1}{\hat{T}_i}\right)\right]\approx\frac{P_{sat}(T_i)}{\sqrt{T_i}}+\frac{P_{sat}(T_i)\left(R_uT_i-2\lambda M\right)}{2R_u\sqrt{T_i^5}}\left(\hat{T}_i-T_i\right) \quad (40)$$

The set of equations of motion at the macroscopic level is the following. For the pair *ji* for j=10 and i=1,2,3,4,5,6 and for *j*=9 and *i*=7,8 (total 7 equations):

$$\delta_i\left(\frac{\hat{\dot{m}}_{ji}-\dot{m}_{ji}}{\Delta t}\psi_1(s_i)+\frac{1}{2}\hat{\dot{m}}_i\,\dot{m}_i\,\psi_2(s_i)=P(s_j^*)-P(s_i)+\hat{\dot{m}}_{ji}\left|\dot{m}_{ji}\right|\int_{s_i^*}^{s_i}\tilde{f}_{iy}(s_i,\mu,A_i)dy_i+\int_{s_i^*}^{s_i}\bar{f}_{iy}dy_i\right) \quad (41)$$

In the above equations, the Boolean factor was shown as multiplier to equation itself rather than its components. It is done in order to underline that a corresponding numerical algorithm should have a feature to eliminate this equation as an object during numerical integration along time, if a specified condition is satisfied.

Figure 4 shows the hydraulic network just after switching from the start-up to normal operation mode, when interfaces *i*=2,3,4 have disappeared (δ_i: 1-->0)

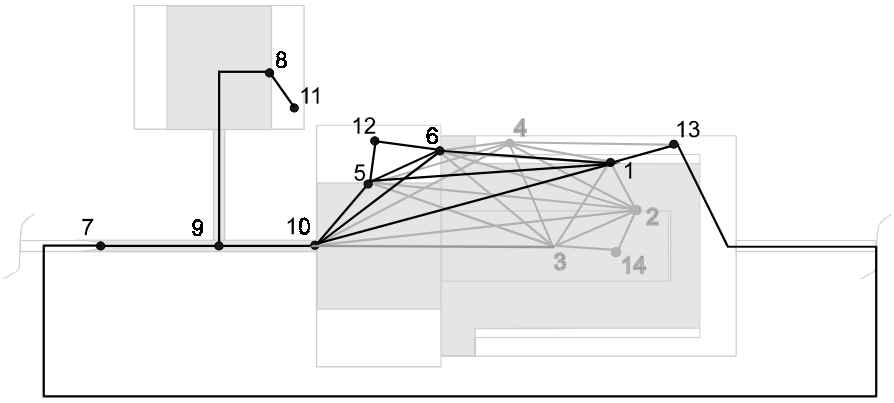

Figure 4. Equivalent hydraulic network for normal mode configuration

Since this moment, the appropriate Boolean variables act as some "sleeping" components controlled by a pre-defined conditions for detection of a bifurcation to another mode, when the previously eliminated interfaces and links may appeared again.

5. Low level model

The equation of motion in the cylindrical coordinates for regions of an evaporator element occupied with liquid phase, in the assumption of viscous incompressible flow is expressed using permeability parameter *K* and porosity ε (Cao and Faghri, 1994). Let set *v* as a velocity along the radius *r* and *w* as an axial velocity along axis Z. These velocities belong to the forward (with respect to positive coordinate direction) boundaries of the grid cell.

$$\frac{\rho}{\varepsilon}\frac{\partial v}{\partial t}+\frac{\rho}{\varepsilon^2}\left(v\frac{\partial v}{\partial r}+w\frac{\partial v}{\partial z}\right)=-\frac{\partial P}{\partial r}-\frac{\mu}{K}v+\frac{\mu}{\varepsilon}\left(\frac{\partial^2 v}{\partial r^2}+\frac{1}{r}\frac{\partial v}{\partial r}+\frac{\partial^2 v}{\partial z^2}-\frac{v}{r^2}\right) \quad (42)$$

$$\frac{\rho}{\varepsilon}\frac{\partial w}{\partial t}+\frac{\rho}{\varepsilon^2}\left(v\frac{\partial w}{\partial r}+w\frac{\partial w}{\partial z}\right)=-\frac{\partial P}{\partial z}-\frac{\mu}{K}w+\frac{\mu}{\varepsilon}\left(\frac{\partial^2 w}{\partial r^2}+\frac{1}{r}\frac{\partial w}{\partial r}+\frac{\partial^2 w}{\partial z^2}\right) \quad (43)$$

In regions where there are no porous structure, ε=1 and K=∞. Mass balance in the liquid bulk is

$$\rho\left(\frac{v}{r}+\frac{\partial v}{\partial r}+\frac{\partial w}{\partial z}\right)=0 \quad (44)$$

The liquid density ρ is a function of temperature *T*, which itself is a function of coordinates *r* and *z* and time *t*. Due to a weak dependence, this relationship can be treated explicitly by a numerical algorithm and in the above equations it appears as a constant.

The energy equations are written as 2D-type for evaporator and reservoirs and as 1D-type for pipelines and condenser. In the evaporator and condenser the equations are applicable to liquid, solid and porous media; the voids are treated as node elements. In the case of division of 3 phases, the latent heat of phase change is applied to the inter-domain boundary from the side of solid media and interpreted as boundary conditions

$$\rho C\frac{\partial T}{\partial t}+\rho C\left(u\frac{\partial T}{\partial r}+w\frac{\partial T}{\partial z}\right)=\frac{1}{r}\frac{\partial}{\partial r}\left(kr\frac{\partial T}{\partial r}\right)+\frac{\partial}{\partial z}\left(k\frac{\partial T}{\partial z}\right) \tag{45}$$

where

$$\rho C=\varepsilon\left[\rho C(1-\varphi)+\varphi\rho''C''\right]+(1-\varepsilon)\rho_w C;\qquad k=k(k,k'',k_w,\varepsilon) \tag{46}$$

For pure solids (i.e. wall and fins of grooves) the equation is similar, but $v=w=\varepsilon=0$.

Boundary conditions for the energy equations are the following. On external surfaces of evaporator or/and reservoir containers the applied heat flux should be specified

$$-k\left.\frac{\partial T}{\partial r}\right|_{r=R}=q(z,t) \tag{47}$$

Conjugation on interfaces at points of 3 phases division are

$$-k\frac{\partial T_w}{\partial \mathbf{n}}=j\lambda-k\frac{\partial T}{\partial \mathbf{n}};\qquad T=T_w \tag{48}$$

At points of two-phase division (vapor-liquid), the equation is similar, but $\partial T_w=0$ and $T_w=T''$.

Equations for pipelines and condenser tube are written for wall and fluid inside:

$$\delta_w C_w\rho_w\frac{\partial T_w}{\partial t}=\delta_w k_w\frac{\partial^2 T_w}{\partial y^2}+\tilde{\eta}q+h(T-T_w)-\varepsilon\sigma\tilde{\eta}T_w^4+\lambda\rho\dot{s}_7\frac{r}{2\Delta y_{eff}}\left[\vartheta(y-s_7)\right] \tag{49}$$

$$\frac{\partial T}{\partial t}=-\frac{\dot{s}_7}{\rho}\frac{\partial T}{\partial y}+\frac{1}{C\rho}\frac{\partial}{\partial y}\left(k\frac{\partial T}{\partial y}\right)+\frac{2h}{rC\rho}(T_w-T) \tag{50}$$

Where η' is a factor accounting the fins area and its effectiveness; $\vartheta(.)$ is a function accounting a distribution of the latent heat of condensation in a region surrounding the imaginary interface position s_7.

Thus, for modeling on the low level, a numerical grid should be established. For evaporator and both reservoirs it can be at least of 2D-type adjusted the geometry; and for pipelines including condenser section is 1D-type. The interaction with higher-level model will be accomplished through the boundary conditions as it shown in the next section.

6. Model interfacing

On all movable interfaces the pressure balance should take place, taking into account the capillary forces

$$P''=\aleph\sigma+P \tag{51}$$

Where $\aleph=\aleph(r,z)$ – local interface curvature and P - local liquid pressure just below the interface. The term "local" means for each control volume of numerical grid. For the interface control volumes, the local mass balance equation looks like

$$\rho\left(\frac{v}{r}+\frac{\partial v}{\partial r}+\frac{\partial w}{\partial z}\right)=\frac{j\ A_{if}\varepsilon}{\Delta V}+\varepsilon(\rho-\rho'')\frac{\partial\varphi}{\partial t} \tag{52}$$

The volumetric vapor quality φ for the control volume ΔV has a relationship with local curvature $\aleph$. The expression depends on the interface shape and peculiarities of capillary structure. For example, if a capillary structure of the evaporator can be represented as a set of cylindrical capillaries of r_p radius, the relationship between φ and $\aleph$ can be obtained as following

$$\varphi = 1 - \frac{\Delta V_{vp}}{\pi r_p^2 h_v}; \qquad \Delta V_{vp} = \pi r_p^3 \Phi_1(\theta)\Phi_2(\theta) + \pi r_p^2 \Delta h_r$$
$$\Phi_1(\theta) = \frac{(1 - Sin\theta)^2}{Cos\theta}; \qquad \Phi_2(\theta) = \frac{(2 + Sin\theta)}{3}; \qquad \aleph = \frac{2Cos\theta}{r_p}, \qquad \theta' \le \theta \le \frac{\pi}{2} \tag{53}$$

The recession Δh_r is equal to 0 for $\theta > \theta'$ and >0 for $\theta = \theta'$. Here, h_v is a height of a CV ΔV and θ' is a minimum wetting angle. Thus, the (54) is a parametric relationship between φ and $\aleph$ through the wetting angle θ, which links (52) and (53). For other types of capillary structures the similar kind relationships can be established.

The average curvature of an interface can be defined from sum of forces acting to the liquid due to surface tensions over whole area of interface. In the assumption that the interface keeps the original shape,

$$\overline{\aleph} = \frac{\sum_k \aleph_k \sigma_k \Delta A_k}{\sigma(\overline{T}) \sum_k \Delta A_k}; \qquad P(s_i) = P'' - \aleph\, \sigma(\overline{T}) \tag{54}$$

Where $P(s_i)$ is a near-interface liquid pressure which is used in the higher-level model; ΔA_k is the area of surface interface element of the control volume.

On system level, the mass balances between moving interfaces (27-33) include components of integral mass flow rates between these interfaces m_{i-j}. These flows should be calculated along streamlines, which begins from *i*-th interface (or *i*-th cross section) and ends at *j*-th interface. This can be performed by a numerical integration on the established numerical grid over 2D CPL components (i.e. evaporator and reservoir). Velocity map yields inter-linked chains of numerical cells, and these chains yields a sequence of projections of imagining streamlines. Note, the streamlines itself are not to be restored; only projections are needed because they are used in the momentum balance equations at low-level modeling.

Therefore, at each time step, for each interface control volume (CV) of *i*-th interface, the sequences of CVs, which belongs to a chain beginning from this CV and ends on the j-th interface, should be defined. It can be accomplished by a recurrent combinatory procedure using current velocity map on numerical grid. The mass flow should be calculated along all found chains and summarized for all chains which link both interfaces, taking into account the accumulating fractions of flow coming along the chain.

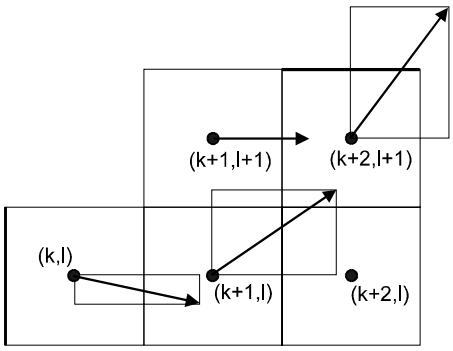

Figure 5. Tangents to a streamline in a velocity map on a numerical grid.

In the Figure 5 let allow the CV *(k,l)* belongs to *i*-th interface and the CV *(k+2,l+1)* belongs to *j*-th interface (gross lines). Current velocity map is displayed. It can be found two chains; first is {*(k,l),(k+1,l),(k+2,l),(k+2,l+1)*} and second is {*(k,l),(k+1,l),(k+1,l+1),(k+2,l+1)*}. The components of the m_{i-j} corresponded to these two chains are

$$\dot{m}_{ij1} = \rho \Delta A w_{(k,l)-(k+1,l)} x_{(k+1,l)-(k+2,l)} x_{(k+2,l)-(k+2,l+1)}$$
$$\dot{m}_{ij2} = \rho \Delta A w_{(k,l)-(k+1,l)} x_{(k+1,l)-(k+1,l+1)} x_{(k+1,l+1)-(k+2,l+1)} \tag{55}$$

Where *w* and *v* are exit velocities from the CV; ΔA is area of the CV side, which correspond to the exit velocity component. Total mass flow from *i* to *j* is

$$\dot{m}_{i-j} = \dot{m}_{ij1} + \dot{m}_{ij2} \tag{56}$$

Numerically, the velocities are defined on boundaries of the grid; in the Figure 5 they are shifted to centers in order to give an idea of streamline tangents behavior.

Fraction of the mass flow rate from a CV "a" to a down-flow neighbor "b" along the defined chain is

$$x_{(a,b)} = \frac{\rho \Delta A u_{(a,b)}}{\sum_{k} (\rho \Delta A u)_{(b,k)}} \tag{57}$$

Where summarizing is performed for all flows exiting the CV. Velocity $u=v \cup w$; first or second has to be chosen in depends of chain path. For general case, the mass flow rate components for the higher-level model are defined as

$$\dot{m}_{i-j} = \sum_{q=1}^{N_{sij}} \dot{m}_{ijq}; \qquad \dot{m}_{ijq} = (\rho \Delta A u)_q \prod_{(a,b) \in SQ_q} x_{a-b} \tag{58}$$

Where N_{sij} is a number of chains exiting the interface (or cross-section) s_i; SQq is a sequence of the (a,b) pairs in the q-th chain.

After obtaining m_{ijq}, the integral hydraulic resistance along the q-th chain can be calculated

$$\begin{aligned} Rh_q = \frac{1}{\dot{m}_{ijq}} \sum_{(a,b) \in SQ_q} & \left[\frac{\mu}{\varepsilon} \tilde{D}_{(a,b)} \left(\frac{\partial^2 v}{\partial r^2} + \frac{1}{r} \frac{\partial v}{\partial r} + \frac{\partial^2 v}{\partial z^2} - \frac{1}{r^2} \right) - \frac{\rho}{\varepsilon^2} \tilde{D}_{(a,b)} \left(v \frac{\partial v}{\partial r} + w \frac{\partial v}{\partial z} \right) - \frac{\mu}{K} v \right] \Delta r_{(a,b)} \\ & + \left[\frac{\mu}{\varepsilon} \tilde{D}_{(a,b)} \left(\frac{\partial^2 w}{\partial r^2} + \frac{1}{r} \frac{\partial w}{\partial r} + \frac{\partial^2 w}{\partial z^2} \right) - \frac{\rho}{\varepsilon^2} \tilde{D}_{(a,b)} \left(v \frac{\partial w}{\partial r} + w \frac{\partial w}{\partial z} \right) - \frac{\mu}{K} w \right] \Delta z_{(a,b)} \end{aligned} \tag{59}$$

Where the operator $\tilde{D}_{(a,b)}(.)$ means the performing of discretization of an argument for the flow between cells a and b in the q-th chain. Finally, the hydraulic resistance along all paths (chains) exiting the interface s_i and coming to interface s_j can be calculated by its components by a formula for parallel branches of a hydraulic network. From the other hand, it is an integral component, defined in the motion equation (41) of the higher-level model

$$Rh_{i-j} = \left| \dot{m}_{ij} \right|^{\alpha} \int_{s_i}^{s_j} \tilde{f}_{iy}(s_i, \mu, A_i) dy_i = \left(\sum_{q=1}^{N_{s_i}} Rh_q^{-1} \right)^{-1} \tag{60}$$

Components of the liquid expansion in the equations (27-33) therefore can be expressed as

$$\Delta \dot{m}_i = \sum_{j \neq i}^{N_n} \sum_{q=1}^{N_{sij}} \sum_{(a,b) \in SQ_q}^{N_{s_i}} x_{(a,b)} \left[\Delta A (\alpha + \beta T) \frac{(\hat{T} - T)}{\Delta t} \Delta y \right]_{(a,b)} \tag{61}$$

Concluding, the interfacing algorithm acts on the following manner. Higher-level model supplies the interface positions for the low-level model. With the frozen interface, the low-level model supplies velocity and temperature distributions over all elements in the system. Based on these magnitudes, the necessary components for the equivalent hydraulic networks are calculated. Then the higher-level model performs a time step to define new positions of the liquid-vapor interfaces. In depends of eventual collapsing or flooding of vapor voids, the structure of equivalent hydraulic network can changed along time integration because of disappearing or appearing the interfaces. The main assumption of such algorithm is that the shapes of interfaces may be predicted a priori, as a function of flooding of voids with liquid.

For numerical stability the time step should be selected to be sensitive to small variations of the curvature of interface (say, to sense the change of meniscus radius to about 10%) at defined rate of evaporation. It is a physical base of the numerical stability. For example, for a capillary structure with a porosity ε and interface capillary radius r_p, when interface is positioned in this structure, the time step is

$$\Delta t \leq 0.1 \frac{r_p \rho A \varepsilon \lambda}{Q_{\max}} \tag{62}$$

For a fine porous structure, used in the CPL evaporator it yields the value of order of 10^{-7} sec. This is a very small time step and it requires significant computer resources. This can correspond to a scale of 10^2 up to 10^3 of real-modeling time for computers with 1GHz 32 bits CPU. But for the conception, which includes the interfaces tracking, it seems inevitable. From other hand, this time step magnitude lies below the possible limit of numerical stability for explicit schemes; that is why the simplified iterative numerical procedures can be applied.

7. Conclusions

A two-level imitation mathematical model has been developed for the hybrid CPL. It includes the macroscopic (system level) and microscopic (component level) models with interacting through moving liquid-vapor interfaces. The main assumption made is that the interfaces are capable to keep its shape when moving; these shapes can be defined a priory in depend of rate of flooding of voids with liquid. In the present configuration these shapes are assumed as cylindrical (interfaces 1,2,5,8), plane ring (interface 6) and cut sphere (interfaces 3 and 6). Modes that can be simulated are the flooded start-up; switch-off by heating of attached reservoir; operation under control of separated reservoir; degradation of performance due to dry-out of evaporator core channel. Numerical algorithm should still be developed.

8. Acknowledgement

The author is very grateful to CNPq organization, Brazil, for the fellowship 300034/96-2 in supporting the research.

9. References

Antoniuk D and Nienberg J., 1998, Analysis of Salient Events from the Two-phase Flow (TPF) Thermal Control Flight Experiment. 28th ICES. Danvers, Massachusetts, July 13-16, SAE Paper 981817, p.1-13.

Butler D, Hoang T., 1991, "The enhanced capillary pumped loop flight experiment: a prototype of the EOS platform thermal control system". Proceedings of the 26th AIAA Thermophysics Conference, Honolulu, AIAA 91-1377.

Butler D, Ottenstein L, Ku J., 1995, "Flight testing of Capillary Pump Loop flight experiment", Proceedings of the 25th International Conference on Environmental Systems, San Diego, CA, SAE Technical Paper Series 951566.

Butler D, Ottenstein L, Ku J., 1996, Design evolution of the Capillary Pumped Loop (CAPL 2) flight experiment. Proceedings of the 26th International Conference on Environmental Systems, Monterey, CA, SAE Paper 961431.

Cao Y, Faghri A, 1994, "Analytical solution of flow and heat transfer in a porous structure with partial heating and evaporation on the upper surface", International Journal of Heat and Mass Treansfer, Vol. 17, N. 10, pp. 1525-1533.

Cullimore, B., Baumann, J., 2000, "Steady-State and Transient Loop Heat Pipe Modeling", Proceedings of the 30th ICES, July 10-13, Toulouse, France. Paper 2000-01-2316, pp. 1-9.

Faghri A, 1995, "Heat pipe Science and Technology", Taylor & Francis

Fugus C, Bray Y.Le, Bories S., Prat M, 1999, "Heat and mass transfer with phase-change in a porous structure partially heated: continuum model and pore network simulation", Int. Journ. Heat and Mass Treansfer, V 42, pp. 2557-2569.

Gerasimov YF, Maidanik YF, Dolgirev YY at al., 1976, "Some results of investigation of low-temperature heat pipes operating against gravity field (in Russian)", Eng.-Phys.J., Vol 30 N 4, pp. 581-586.

Hoang T, Ku J., 1995, "Theory of hydrodynamic stability for capillary pumped loops", Proceedings of the ASME National Heat Transfer Conference, Portland, Oregon, Vol. 5, p. 33-40.

Khrustalev D, Faghri A., 1995, "Heat transfer in the inverted meniscus type evaporator at high heat fluxes", International Journal of Heat and Mass Treansfer, Vol. 38, N 16, pp. 3091-3101.

Kiper AM., Swanson TD, McIntosh R., 1988, "Exploratory study of temperature oscillations related to transient operation of a capillary pumped loop heat pipe", Proceedings, ASME Nat. Heat Transfer Conf., Houston, p.353-359.

Kolos KR, Herold KE., 1997, "Low frequency temperature and fluid oscillations in Capillary Pumped Loops", Proceedings of National Heat Transfer Conference, Baltimore, MD, paper AIAA 97-3872.

Ku J, Hoang T., 1995, "An experimental study of pressure oscillation and hydrodynamic stability in a Capillary Pumped Loop", Proceedings of the ASME National Heat Transfer Conference, Portland, Oregon, vol. 5, p. 25-32.

Ku J, Ottenstein L, Butler D., 1996, "Performance of CAPL 2 flight experiment", Proceedings of the 26th International Conference on Environmental Systems, Monterey, CA, SAE Paper Series 961432.

Ku J., 1999, "Operating characteristics of loop heat pipes". SAE Paper 99012007. Proceeding of the 29th International Conference on Environmental Systems. July 12-15, Danvers (Massachusetts, USA), pp. 1-16.

Maidanic YF, Fershtater YG., 1997, "Theoretical basis and classification of loop heat pipes and capillary pumped loops", Proceeding of the 10th International Heat Pipe Conference. September 21-25, Stuttgart (Germany), pp. 1-15.

Maidanik Y, Fershtater Y, Pastukhov VG, Chernysheva M., 1993, "Experimental and theoretical investigation of startup regimes of two-phase capillary pumped loops", Proceedings of the 23rd International Conference on Environmental Systems, Colorado Springs, CO, SAE Technical Paper Series 932305.

Maidanik YF, Vershinin S, Kholodov V, Dolgirev J., 1985, "Heat Transfer Apparatus", US Patent, May 7, No. 4515209

Muraoka I., Vlassov VV, 2000, "Numerical Model of the CPL for Microgravity Experiment", Preprint of the 6th International Heat Pipe Symposium - 6IHPS-2000, 5-9 November 2000, Chiang Mai, Thailand, pp.105-112.

Nikitkin M, Cullimore B., 1998, "CPL and LHP tekhnologies: what are the differences, what are the similarities", SAE Paper 981587. Proceeding of the 28th ICES. July 13-16, Danvers (Massachusetts, USA), pp. 1-10.

O'Connell T, Hoang T, Ku, J., 1995 "Investigation of power turn down transients in CAPL-1 flight experiment", Proceedings of the 30th AIAA Thermophysics Conference, San Diego, CA, paper AIAA 95-2067.

Stenger F.J., 1966. "Experimental feasibility study of water-filled capillary-pumped heat- transfer loops", Washington, D.C., NASA, 1966, NASA TM X-1310.

Wolfram, S., 1991, “Mathematica”, Addison Wesley.